

RESEARCH

Open Access



# Exploring the viability of combined laser-induced breakdown spectroscopy and Raman spectroscopy for stratigraphic analysis of murals containing isomeric pigments: a case study on realgar and orpiment

Duixiong Sun<sup>1</sup>, Hanyun Li<sup>1</sup>, Guoding Zhang<sup>1</sup>, Yaopeng Yin<sup>2\*</sup>, Maogen Su<sup>1</sup>, Xueshi Bai<sup>3</sup>, Marek Sikorski<sup>4</sup> and Denghong Zhang<sup>1\*</sup>

## Abstract

A novel combined measurements techniques has been designed in this work, enabling the acquisition of laser-induced breakdown spectroscopy (LIBS) and Raman spectral signals at the same point on a sample. The application of this combined technique to the analysis of multi-layered mock-up blocks painted with orpiment and realgar pigments has yielded significant insights. By correlating variations in the emission line intensity of characteristic elements within the LIBS spectra with depth-specific Raman spectra, the number of laser pulses that penetrated the pigment layers has been accurately determined, thereby establishing a method to measure layer thickness. Finally, the technique wasto analysis the actual mural fragment from Mogao Cave 196, determining the types of pigment and the thickness of the pigment layers.

**Keywords** Mogao Grottoes, Wall paintings, Laser-induced breakdown spectroscopy, Raman spectroscopy, Orpiment, Realgar

\*Correspondence:

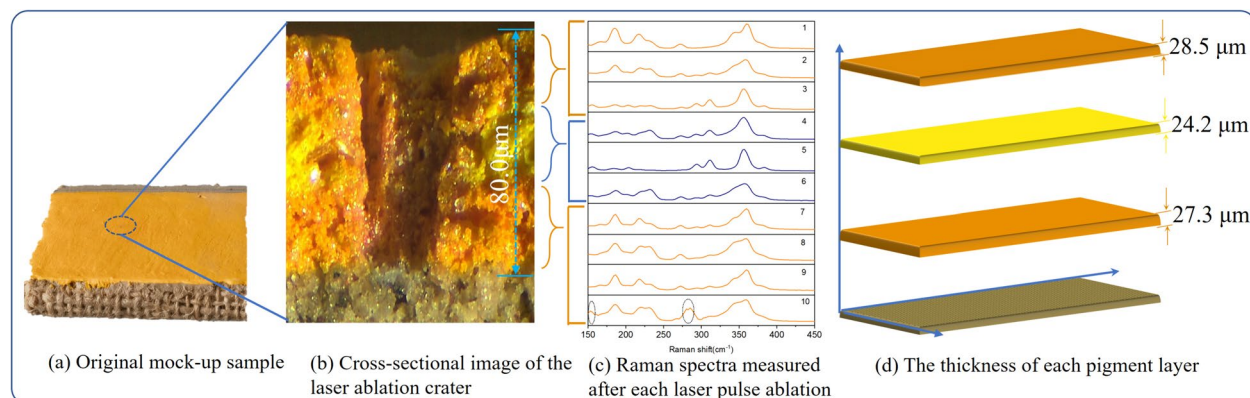
Yaopeng Yin  
yiny@dh.ac.cn  
Denghong Zhang  
zhangdh@nwnu.edu.cn

Full list of author information is available at the end of the article



© The Author(s) 2024. **Open Access** This article is licensed under a Creative Commons Attribution 4.0 International License, which permits use, sharing, adaptation, distribution and reproduction in any medium or format, as long as you give appropriate credit to the original author(s) and the source, provide a link to the Creative Commons licence, and indicate if changes were made. The images or other third party material in this article are included in the article's Creative Commons licence, unless indicated otherwise in a credit line to the material. If material is not included in the article's Creative Commons licence and your intended use is not permitted by statutory regulation or exceeds the permitted use, you will need to obtain permission directly from the copyright holder. To view a copy of this licence, visit <http://creativecommons.org/licenses/by/4.0/>. The Creative Commons Public Domain Dedication waiver (<http://creativecommons.org/publicdomain/zero/1.0/>) applies to the data made available in this article, unless otherwise stated in a credit line to the data.

## Graphical Abstract



## Introduction

The Mogao Grottoes in Dunhuang, situated in China's Gansu province, constitute a significant portion of cultural heritage dating back to the pre-Qin dynasty, over 1600 years ago. As a global pinnacle of Buddhist art, the site encompasses over 2000 painted sculptures, approximately 735 caves and murals spanning over 45,000 square meters [1–3]. Recognized by UNESCO as a World Heritage site in 1987, the Mogao Grottoes stand out for their rich cultural narratives, artistic mastery, and the sheer magnitude of their mural collections. Using the dry fresco or *secco* technique, Dunhuang artists applied vibrant mineral pigments mixed with organic binders to create murals with varied hues and brightness. In the context of these multilayered murals, it is crucial to accurately analyze the composition and thickness of individual pigment layers within the paintings. This analysis is essential as these murals are susceptible to deterioration, including flaking, discoloration, and structural damage, et al. [4]. Consequently, preservation and conservation efforts necessitate the use of non-destructive or minimally invasive techniques, ideally suited for on-site application.

In the field of cultural heritage conservation, laser-induced breakdown spectroscopy (LIBS) has emerged as a valuable technique for rapid elemental analysis of painted surfaces, particularly murals. Its advantages include ease of operation, minimal sample preparation, and negligible impact on artwork, making it ideal for *in situ* analysis [5–7]. LIBS functions by focusing a laser on the artwork, generating plasma and analyzing the emitted atomic and ionic spectra [8, 9]. Importantly, LIBS enables depth profiling, also known as LIBS stratigraphy. This involves sequential laser ablation to examine individual pigment layers [10–15]. By collecting elemental composition data at various depths, LIBS provides a

layered analysis of the artwork. Each laser pulse produces a depth-specific plasma, allowing for the collection of spectral data [16, 17]. However, LIBS may be limited to analyzing pigment layers with uniform elemental compositions. In such cases, complementary molecular analysis techniques such as Raman spectroscopy are necessary for comprehensive material characterization [14, 18–21].

Raman spectroscopy, a vibrational spectroscopy technique, facilitates the detection of the molecular structure of samples by analyzing the energy change resulting from inelastic scattering when a laser interacts with the sample [22]. Widely adopted in archaeological cultural relic research, Raman spectroscopy offers notable advantages such as the non-requirement of sample preparation, non-contact detection, complete non-destructiveness of the sample, and high spatial resolution [23–31]. However, a significant drawback is the limited penetration depth of excitation light, which hinders the acquisition of Raman signals from deeper sample layers [32].

To address this limitation, the combination of LIBS technology and Raman spectroscopy emerges as a promising approach, offering distinct yet complementary information for the layer-by-layer analysis of multilayer pigment murals. Numerous studies have demonstrated the synergistic application of these technologies in the investigation of multilayered cultural relics and artworks [33–39]. Castillejo et al. [38], for example, successfully used LIBS and Raman technology to identify pigments on an altar of the eighteenth century of the Museum of Zaragoza, Spain. Romain et al. [35] employed a combination of LIBS and Raman measurement spectra to address the analysis of the thickness of green pigments. Veneranda et al. [39] applied LIBS and Raman techniques to analyze frescoes at a site in Pompeii, Italy, assessing salt damage and discussing the fading mechanism based on

combined spectral data. Although studies have effectively combined LIBS and Raman techniques for cultural artifact analysis [40], because of surface contaminants, oxidation products, or the presence of salts can significantly affect the results of LIBS and Raman [41], further development of combined technique between LIBS and Raman is needed that focuses specifically on layer-by-layer analysis of murals painted with pigments that share the same elemental composition.

Orpiment ( $\text{As}_2\text{S}_3$ ) and realgar ( $\text{As}_4\text{S}_4$ ) composed by elements arsenic and sulfide, both of which have the same constituent elements and similar structures, and have a long history of use in ancient China, and this pigments were widely used in Dunhuang Murals. Realgar exhibits a reddish-yellow hue, while orpiment is a pure, bright yellow. In Dunhuang murals, these two pigments are typically used in an overlapping shading technique to represent different shades. Overlapping shading is a technique used in traditional cave painting. It involves creating two to four shades from the same color or similar colors and then arranging and painting them sequentially. For instance, a layer of realgar might be applied over orpiment, or vice versa, or multiple layers of each might be used. By carefully controlling the thickness of each pigment layer, artists achieved nuanced shades of yellow, resulting in murals with a complex, multilayered structure composed of these pigments. Therefore, the analysis of multilayer pigment murals composed of orpiment and realgar can reveal crucial insights into painting techniques, as well as trace the variations in material use and production processes of yellow pigments in ancient murals. However, research on orpiment and realgar pigments in Dunhuang murals remains limited. In 2008, Yu et al. [42] conducted an analysis of yellow pigments in two caves by using micro-area X-ray fluorescence combined with microscopy and electron microscopy-energy dispersive spectroscopy analysis methods, identifying them as arsenic and sulfur compounds. While this led to a preliminary presumption of realgar or orpiment usage, the study could not definitively distinguish between the two pigments.

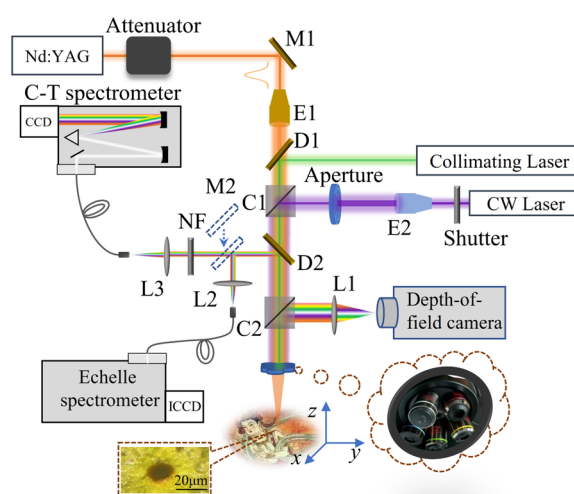
In this work, we developed a novel combined measurement technique to obtain LIBS and Raman spectral signals at the same point on a sample. This technology was applied to investigate multilayered murals painted with orpiment and realgar pigments, which are difficult to distinguish in the Dunhuang murals. Our experimental protocol involved cyclic detection. First, LIBS was used to ablate a thin layer of pigment and capture atomic spectra. Next, a CW laser was used for Raman detection. Following the acquisition of the Raman signal, LIBS detection was performed again at the same point. By analyzing variations in the emission line intensity of characteristic

elements within the LIBS spectra, we determined the number of laser pulses that penetrated the pigment layers, corresponding to layer thickness. Depth-specific Raman spectra were simultaneously acquired. Additionally, a computational depth-of-field camera measured the depth of the ablated crater after each laser pulse, establishing a relationship between the number of laser pulses and sample depth.

## Experimental setup and samples

### Experimental setup

The schematic diagram of the combination of the LIBS and Raman experimental setups is shown in Fig. 1. Both LIBS and Raman detection are operated in open air. An Nd:YAG laser (Beamtech, Dawa-100) outputs 1064 nm light, which mirror M1 directs into a 30 mm cage assembly. An expander E1 ensures uniform beam energy distribution before the beam passes through components dichroic mirror D1, beam-splitter cube C1, dichroic mirror D2, and beam-splitter cube C2. A 10× microscope objective focuses the laser onto the sample surface, generating plasma. The plasma radiation is collimated by the same objective and reflected by dichroic mirror D2 and shifting mirror M2 into an optical fiber. This fiber guides the radiation to a high-resolution spectrometer (Aryelle-200, LTB), and the spectra are recorded by ICCD detector (PI Max-400, Princeton Instrument) for analyzing. The resolving power and spectral range of the spectrometer are 10 000 and 200–800 nm, respectively. Each LIBS ablation



M1, M2: Mirror; D1, D2: Dichroic mirror; E1, E2: Expander; L1, L2, L3: Lens; NF: Notch filter

**Fig. 1** Schematic of experimental setup to combine of the laser-induced breakdown spectroscopy (LIBS) and Raman spectroscopy

crater can be measured by a 3D computational depth-of-field camera (Tmetrics C20, Tucsen Photonics).

For Raman measurement, a 785 nm CW laser beam follows a similar optical path and is focused into the ablation crater. Expander E2 and an aperture were used to improve the uniformity and reduce the size of the laser beam. This resulted in a focused spot smaller than the LIBS crater, facilitating convenient alignment of the Raman laser beam within the LIBS crater. The shifting mirror M2 will be removed from the optical path during Raman measurement. Raman signal is collected via optical fiber and transmitted to a Czerny-Turner spectrometer (Shamrock SR-500i, Andor tech.). The collimating laser and the Raman laser are precisely aligned to completely overlap after reflection (the positions of the two focal points are determined using a depth-of-field camera). After the LIBS measurement, the collimating laser can confirm whether the Raman laser is focused on the LIBS ablation crater.

For the whole LIBS experiment, the sample is fixed on an XYZ-3D linear stage, and the spectrometer, laser and 3D linear stage are synchronized by a digital delay generator (DG535, Stanford Research Systems).

### Samples

To replicate the appearance of Mogao Grottoes murals, a mock-up sample was created using the secco technique [3]. This study focuses on two pigments, orpiment ( $\text{As}_2\text{S}_3$ ) and realgar ( $\text{As}_4\text{S}_4$ ). The pigments were sourced from Lhasa, Tibet and prepared according to traditional mineral processing methods. A 5% gelatin solution was prepared by dissolving 2 g of gelatin powder in 40 mL of deionized water and heating in a water bath. The solution

was then mixed with 2 g of each pigment and applied to the ground layer.

In order to perform stratigraphic analysis, multilayered pigment samples were created, as shown in Fig. 2. A white gypsum base layer was applied to the plaster, followed by yellow pigment layers of varying thickness. Layers were applied in ascending order from bottom to top: realgar, orpiment, and then realgar. Ten samples with different pigment thicknesses were produced;  $d_1$  to  $d_{10}$  represents a gradual increase in the thickness of each layer. As can be seen in Fig. 2, different pigment thicknesses can also result in significant differences in color tone. The gelatin solution acts as an adhesive and as a fixative, ensuring the longevity of the mural [43].

## Results and discussion

### LIBS and Raman analysis on surface pigments

The identification of pigments on the mural surface is crucial for their protection and restoration. However, with the deterioration of murals, it has been difficult to identify pigments with similar colors directly from their color tones, such as realgar and orpiment. Therefore, we have first attempted to use LIBS technology to distinguish these two mineral pigments. Figure 3 presents typical LIBS spectra for orpiment and realgar in the wavelength range of 220–800 nm. Analysis has revealed nearly identical elemental compositions for both yellow pigments, including As, Fe, Mg, and Ca. In addition to As, these elements primarily originate from associated minerals within the pigments. Since orpiment and realgar are both low-temperature hydrothermal minerals, they often form in proximity within low-temperature hydrothermal deposits and sulfurous

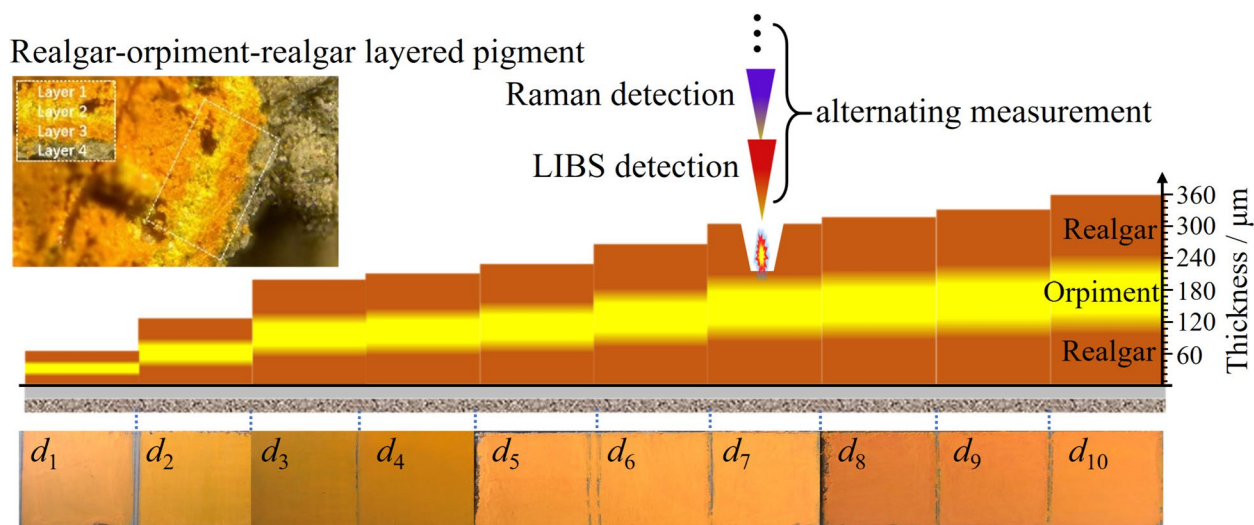


**Fig. 2** Schematic diagram of samples with different painted layer thicknesses. The top left image is a cross-sectional photo of the mock-up sample, which clearly shows the different layer structures

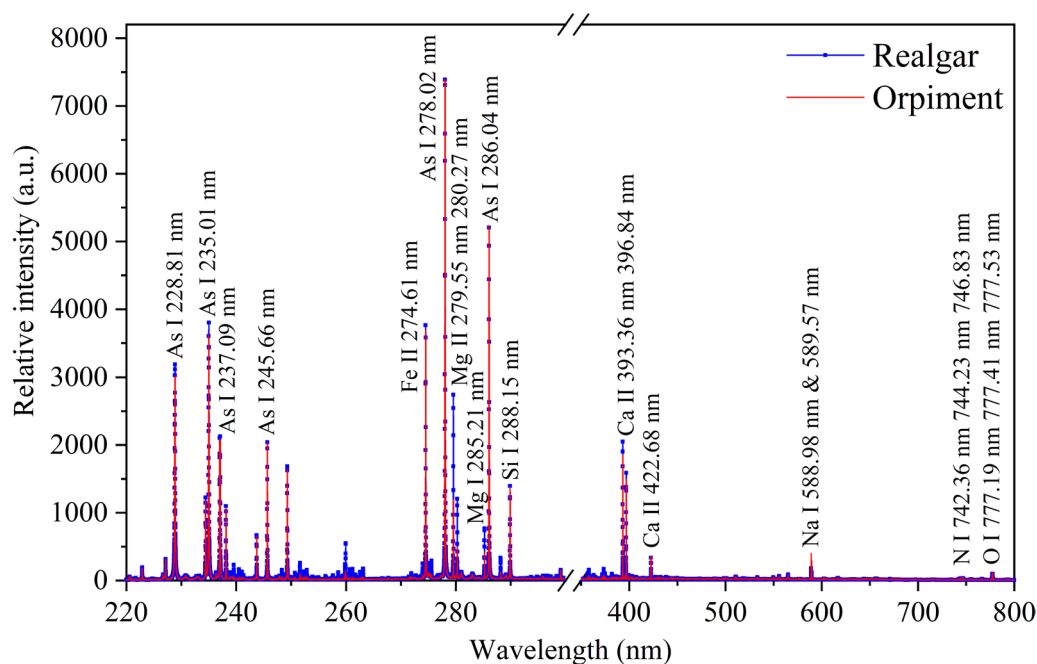


**Fig. 3** Typical LIBS spectra of orpiment and realgar representative samples

volcanic vents. This shared genesis has resulted in a high degree of similarity in both the content and types of trace elements found within these two mineral pigments. In particular, characteristic arsenic lines are identical between pigments, making differentiation based on spectral data alone impossible. Moreover, the close similarity between orpiment and realgar LIBS spectral intensities has further hindered identification efforts. Looking for an alternative approach, we have attempted to correlate spectral data for other detected elements (Mg, Si, Fe, Ca) to differentiate orpiment and realgar. However, this has been unsuccessful. The inherent presence of mineral impurities and the relatively low purity of these natural minerals pose a significant challenge to rely solely on impurity minerals for reliable identification.

PCA-based chemometrics has shown significant advantages in clustering LIBS spectral data [44]. Therefore, we attempted to analyze the LIBS spectra of two yellow pigments using PCA. However, mineral pigments used in murals often have particle sizes ranging from tens to hundreds of micrometers [45], this size is comparable to the laser spot focused in LIBS measurements, leading to spectral instability due to surface roughness. Additionally, fluctuations in laser energy and optical system jitter can exacerbate this effect. The spectral data was preprocessed before performing PCA analysis. To analyze the spectral stability, 100 spectra were collected from mock-up murals with orpiment

and realgar-layered surface. The characteristic lines of As I 228.81 nm, As I 235.01 nm, As I 278.02 nm, As I 286.04 nm and Ca II 393.36 nm were selected. Relative standard deviations (RSDs) of the 100 spectra were calculated for both pigments before and after normalization, as shown in Fig. 4. Three normalized methods were utilized to perform normalization, total area normalization, maximum value normalization and Min–Max normalization [46]. It can be seen that unnormalized data showed significantly higher RSDs for characteristic emission lines. After normalization, the RSDs were reduced, and the Min–Max method demonstrates the most pronounced decrease. Therefore, subsequent spectral analyzes will utilize Min–Max normalization.

A PCA cluster model has been constructed using 200 LIBS spectra from orpiment and realgar mock-up samples. After normalization, 42 emission lines (As, Si, Fe, Ca, Mg, Na) have served as input variables. Figure 5 shows the 2D PCA score plot. PC1 and PC2 explain 85.8% of the variance (PC1: 76.2%, PC2: 9.6%) and sufficiently represent the data. The two types of pigment data sets cluster roughly into separate groups based on PC1 and PC2 scores. However, approximately 28% of the data overlap, making clear separation impossible. This implies that LIBS is ineffective in identifying these yellow pigments on murals. The main cause, as previously stated, is the similarity of accessory minerals in the pigments, rendering PCA-based clustering

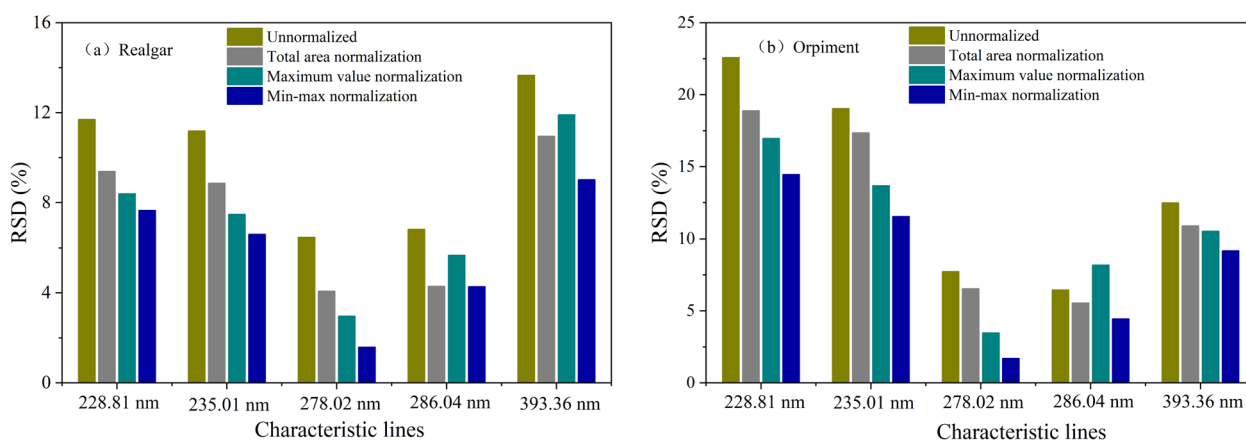


**Fig. 4** The relative standard deviation (RSD) of characteristic spectral line intensity before and after the normalization of LIBS spectral signal in the **a** realgar and **b** orpiment pigment layer

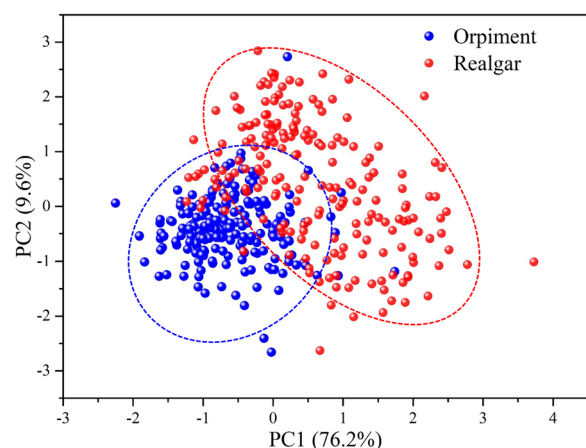


**Fig. 5** Score plots of PC1 and PC2 for characteristic LIBS lines of orpiment and realgar on the mock-up samples

ineffective regardless of macro- or micro-element analysis.

Although realgar and orpiment share the same elemental composition, their distinct molecular structures make Raman spectroscopy a promising technique for their discrimination. Raman spectra result from inelastic light scattering, a process sensitive to the vibrational modes of molecular bonds. However, direct in situ Raman measurements on murals face challenges due to strong fluorescence interference from organic protective layers and surface dust [47]. To address this, we performed Raman measurements within ablation craters previously created by LIBS using single-laser pulses. Figure 6 presents the Raman spectra (150 to 450  $\text{cm}^{-1}$ ) of realgar and orpiment measured from the crater bottoms. Significant differences in band positions and intensities are evident, which facilitates mineral identification. For clarity, the spectra

are divided into two regions: (a) 150–250  $\text{cm}^{-1}$  (S-As-S bending modes) and (b) 250–450  $\text{cm}^{-1}$  (As-S stretching vibrations). Table 1 summarizes the Raman shifts and corresponding vibrational modes for each mineral [48]. These results demonstrate the ability of Raman spectroscopy to successfully distinguish these mineral pigments. When applied to multi-layered murals containing both orpiment and realgar, the combination of LIBS and Raman technologies offers the potential to reveal stratigraphic information.

#### Stratigraphic analysis of murals

This section employs LIBS to investigate the stratigraphy of wall paintings under sequential laser ablation. The stratigraphic analysis protocol is as follows: The mock-up samples displayed a distinct boundary between the yellow pigment layer and the base layer. The significant differences in composition between these layers allow for clear differentiation. Since Ca and As are predominant elements in gypsum and yellow pigment, respectively, the lines of Ca II 393.36 nm and As I 286.04 nm were chosen as indicators for the gypsum base layer and yellow pigment layer. We could determine the number of laser pulses to penetrate the pigment layer by monitoring variations in the selected characteristic line intensities. However, as seen in Fig. 3, natural orpiment and realgar minerals contain associated minerals with Ca elements, which can interfere with measurements. To address this, solid samples were created using orpiment and realgar mineral pigments mixed with glue. Following the scheme described previously, LIBS measurements were performed on these samples to inspect the intensity ratio of Ca II 393.36/As I 286.04 as a function of laser pulse number, as shown in Fig. 7. It clearly shows that the value of intensity ratio is always around  $0.625 \pm 0.15$  both

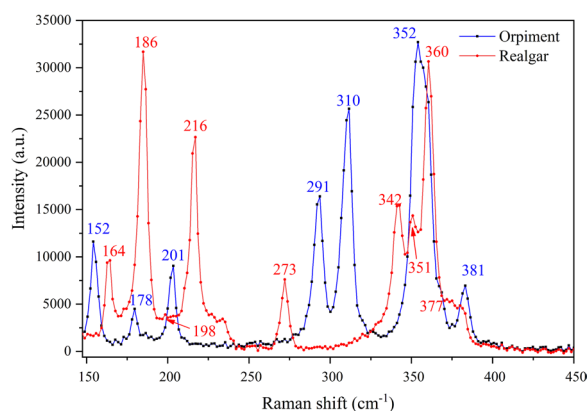


**Fig. 6** Raman spectra of orpiment and realgar of selected samples

for orpiment and realgar in the two pure pressed tablets of yellow pigments, this implies that the plasma generated by LIBS satisfies stoichiometric ablation as the ablation depth increases. Consequently, it is possible to infer whether the laser penetrates the pigment layer by analyzing the changes in the ratios of monitored spectral line intensities.

Depth analysis was conducted on samples with pigment thicknesses ranging from  $d_1$  to  $d_{10}$ . The results demonstrate that continuous laser ablation at the same point leads to a gradual weakening of As spectral lines and a corresponding strengthening of Ca spectral lines. Notably, the ratio of Ca II 393.36/As I 286.04 spectral line intensity offers a more sensitive indicator for determining the number of laser pulses required for penetration of the pigment layer. As illustrated in Fig. 7, a Ca II 393.36/As I 286.04 ratio exceeding 0.725 suggests successful laser penetration of the pigment layer.

Figure 8 shows the results of the analysis in the sample with thicknesses  $d_1$  to  $d_{10}$ . Considering the sample with thickness  $d_1$  as an example for analysis; the observed change in the Ca II 393.36/As I 286.04 ratio indicates that the penetration of the pigment layer occurred at the 10th laser pulse. Due to the Gaussian beam profile of the laser, the energy is highest at the focal spot's center.

Consequently, the higher ablation rate at the beam's center vaporizes the base layer material, whereas lower-energy regions at the beam wings induce some additional signal contribution from the yellow layer boundary. As ablation progresses, the entire focal point is penetrated. To verify whether the laser pulse penetrated the pigment layer at a specific laser pulse, the ablation craters produced after the 30th laser pulse were measured using a computational depth-of-field camera. The morphology of the ablation crater is shown in Fig. 8 as inserts. As can be seen clearly in the inserts, the base layer was detected with off-white was detected at the bottoms of the craters, and this agrees with the variations in characteristic element intensities in the pigment layer from vanishing. In addition, the interaction between the expanding plasma and the crater wall prevents the characteristic element intensities in the pigment layer from vanishing. Therefore, the dominant spectral lines observed after the 20th pulse ablation primarily originate from the Ca in the base layer.

For samples with realgar pigment thicknesses ranging from  $d_2$  to  $d_{10}$ , the number of laser pulses required to initiate penetration progressively increases (19, 25, 30, 35,

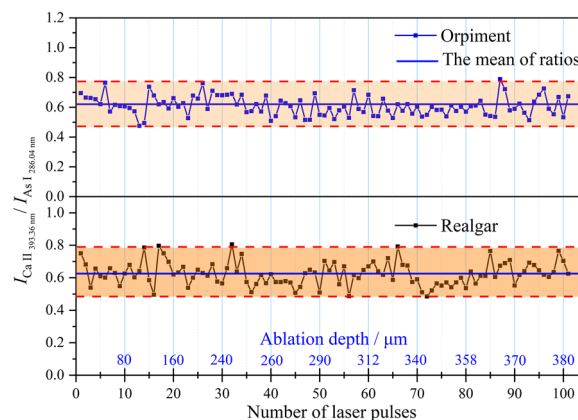


**Fig. 7** The intensity ratio of Ca II 393.36/As I 286.04 as a function of laser pulse number. The solid blue lines represent the mean of ratios (0.625). It should be noted that while the number of laser pulses changes linearly, the ablation depth does not change linearly

**Table 1** Raman spectra and corresponding vibration mode of orpiment ( $As_2S_3$ ) and realgar ( $As_4S_4$ ) [46]

Orpiment ( $As_2S_3$ )		Realgar ( $As_4S_4$ )	
Raman shift ( $cm^{-1}$ )	Assignment	Raman shift ( $cm^{-1}$ )	Assignment
201	As-S-As bending variation	164,216	As-As-S bending variation
152	As-As-S bending variation	186	As-S-As bending variation
178	S-As-S bending variation	198	As-As stretch
291,310	As-S antisymmetric stretch	273	As-S bending variation
352	As-S stretch	342,351,360	As-S stretch
381	As-S-As stretch	377	S-As-S stretch

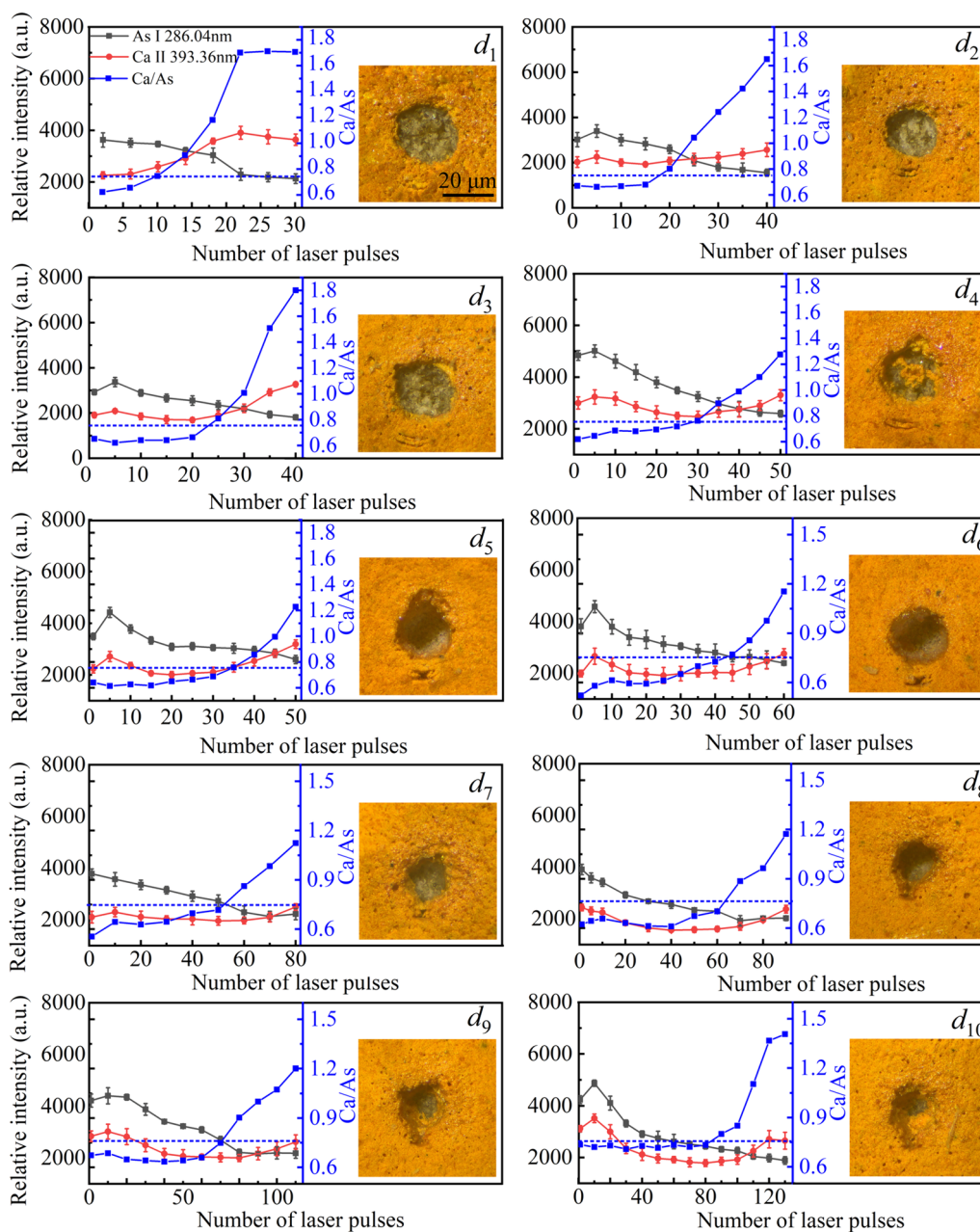


**Fig. 8** The intensities of two spectral lines, Ca II 393.36 nm and As I 286.04 nm, along with the variation of their intensity ratio as a function of the number of laser pulses. The blue dashed line represents the threshold. If the intensity ratios of the two spectral lines exceeds this value, it indicates that the laser has penetrated the paint by realgar layer. Samples  $d_1$  to  $d_{10}$  correspond to pigment layers with increasing thicknesses. The insets on the right of each image are the morphologies of the corresponding ablation craters captured using a computational depth-of-field camera after laser ablation complete

45, 55, 67, 72, and 85 pulses, respectively). Additionally, the ablation craters obtained by a computational depth-of-field camera reveal a trend toward a conical shape as the pigment layer thickness increases. This structure aligns perfectly with the behavior of a Gaussian laser beam profile.

We measured the depths of ablation craters for 10 samples at specified numbers of laser pulses with a computational depth-of-field camera; for samples  $d_1$  to  $d_{10}$ , the thicknesses of the total pigment layers are 80.2, 163.4, 210.2, 235.3, 246.2, 278.1, 300.7, 333.2, 345.4, and 360.5  $\mu\text{m}$ , respectively. Meanwhile, the average

ablation rates at different thicknesses were calculated by dividing the ablation crater depth by the number of laser pulses, as shown in Fig. 9. It can be seen that the depth of the ablation craters increases with continuous laser ablation. Initially, during the first 30 pulses, the depth of the crater exhibits a linear relationship with the number of laser pulses. However, as ablation continues, the rate of increase in crater depth gradually decreases. This trend is also approved in the average ablation rate, which decreases after the 30th pulse, signifying a decline in the material removal efficiency of each laser pulse. The primary reason for this is that, as the ablation depth increases, the laser power reaching the bottom of the craters decreases under a constant focusing system. Additionally, the ablation craters constrain the plasma, causing a portion of the ablated material to return to the bottom of the crater. Despite the declining ablation rate, this fixed-focus optical design demonstrates sufficient capability to penetrate the pigment layers and complete stratigraphic analysis. This is essential for examining the layer-by-layer structure of pigments.

Following each laser pulse ablation for LIBS measurements, Raman spectroscopy was performed directly on the crater bottoms. This approach established a one-to-one correspondence between the LIBS-measured depths

and the associated Raman spectra. As shown in Fig. 10, the red curves represent the Raman spectra obtained from the sample surfaces, corresponding to the realgar reference spectrum. The notation " $d_1$ -2" signifies the Raman spectrum acquired at the bottom of the crater formed on sample  $d_1$  after two laser pulse ablations. Similarly, " $d_2$ -2" denotes the Raman spectrum acquired at the bottom of the crater formed on sample  $d_2$  after two laser pulse ablations, and so on. To enhance clarity, only Raman spectra obtained after specific laser pulse ablations are presented for each sample in the figure.

For sample  $d_1$ , compared to the surface Raman spectrum (red curve), the green and pink spectra (2nd and 8th laser pulse ablations, respectively) structures are very similar to it, the difference being the appearance of characteristic peaks from the orpiment at 291 and 310  $\text{cm}^{-1}$ . As previously mentioned, the Gaussian beam profile of the laser results in conical ablation craters. Due to the spot size of the Raman laser of approximately 10  $\mu\text{m}$ , when focused at the bottom of the craters, the acquired Raman spectrum encompasses all substances within that diameter. Consequently, when the surface pigment layer is initially breached, the spectrum will exhibit characteristic peaks of both orpiment and realgar. Following the second laser pulse ablation, the emergence of weak peaks at 291  $\text{cm}^{-1}$  and 310  $\text{cm}^{-1}$  in the measured Raman

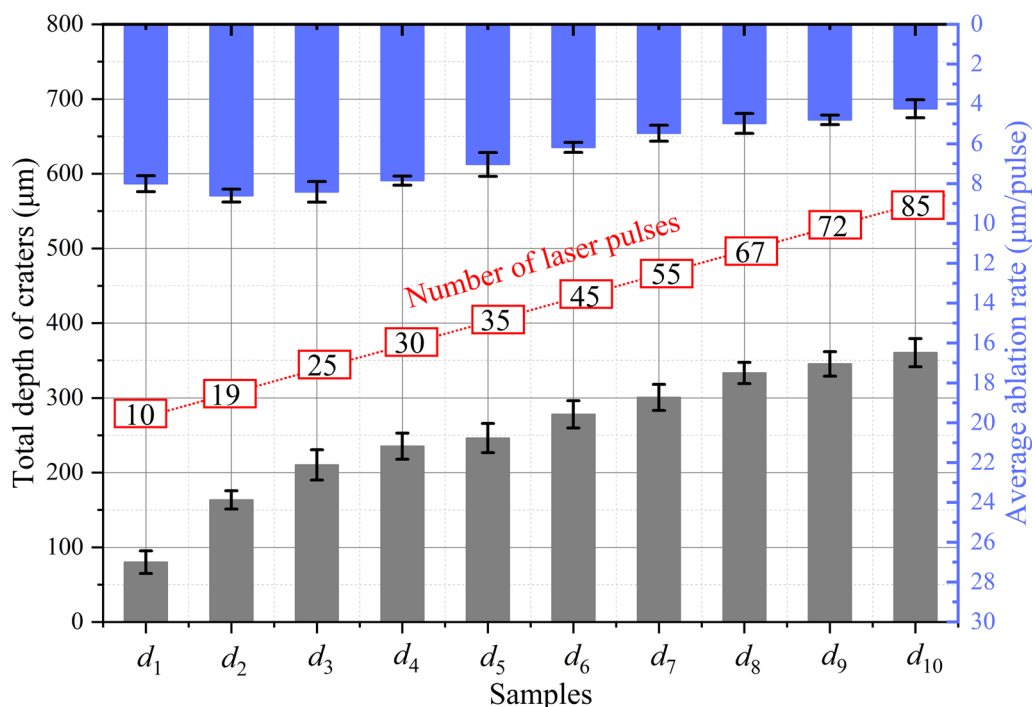


**Fig. 9** The depth of the laser ablation craters on samples  $d_1$  to  $d_{10}$ . The numbers inside the red box represent the corresponding number of laser pulses when the pigment layer was just penetrated, while the bar chart at the top represents the average ablation rate at this number of laser pulses. The error bars represent the standard deviation of ten measurements

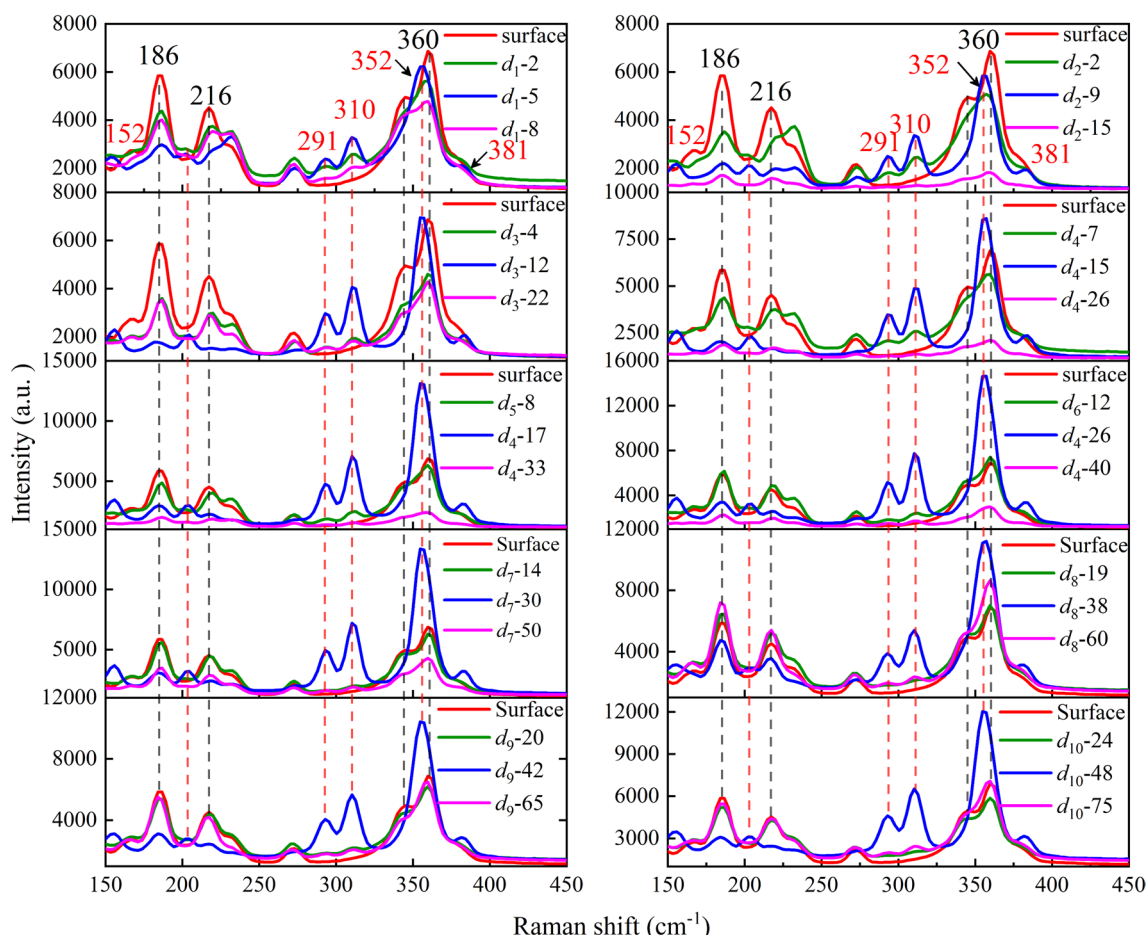


**Fig. 10** Raman spectra of realgar pigment layers from samples  $d_1$  to  $d_{10}$  under different numbers of laser ablations. The notation " $d_1-2$ " signifies the Raman spectrum acquired at the bottom of the crater formed on sample  $d_1$  after two laser pulse ablations. Similarly, " $d_2-2$ " denotes the Raman spectrum acquired at the bottom of the crater formed on sample  $d_2$  after two laser pulse ablations, and so on

spectrum signifies the penetration of the realgar surface layer, revealing the presence of orpiment. However, after the 5th laser pulse ablation (blue line), the strong lines at  $291\text{ cm}^{-1}$ ,  $310\text{ cm}^{-1}$ , and  $352\text{ cm}^{-1}$  become prominent, signifying the domination of the orpiment. Similar trends are observed for samples  $d_2$  to  $d_{10}$ . This demonstrates that Raman spectroscopy effectively distinguishes between orpiment and realgar based on the characteristic Raman shifts under different laser pulse ablation conditions, offering an advantage over LIBS in this regard.

Based on the characteristic changes in the Raman spectra and the number of laser ablation pulses, we can measure the thickness of each pigment layer using a 3D computational depth-of-field camera, as shown in Table 2. This thickness matches very well with the painting techniques employed during the creation of our samples.

### Stratigraphic analysis on actual mural fragment

Based on the successful application of LIBS and Raman analysis to mock-up samples, this experimental protocol was applied to an actual mural fragment. The fragment was collected from a deteriorated section of the north wall in Cave 196 of the Mogao Caves.

Cave 196, also known as the He Fashi Cave, was constructed during the Jingfu period of the late Tang Dynasty (892–893 AD). This cave comprises a front chamber, passageway, and main chamber. The front chamber features a distinctive eave structure, while the square main chamber houses a central Buddha altar with a screen connecting it to the ceiling. The cave's murals depict scenes from various Buddhist sutras: the Golden Light Sutra, Amitabha Sutra, and Lotus Sutra on the south wall; the Maitreya Sutra, Medicine Buddha Sutra, and Avatamsaka Sutra on the north wall; the Lāṭṭavistara Sūtra on the

**Table 2** The thickness of each layer of orpiment and realgar in samples  $d_1$  to  $d_{10}$

Samples	Thickness ( $\mu\text{m}$ )									
	$d_1$	$d_2$	$d_3$	$d_4$	$d_5$	$d_6$	$d_7$	$d_8$	$d_9$	$d_{10}$
Layer 1(realgar)	28.5	50.2	68.2	75.2	75.2	90.2	102.5	105.3	117.3	125.3
Layer 2(orpiment)	24.2	58.4	74.3	80.6	86.3	95.6	94.3	118.6	112.2	115.5
Layer 3 (realgar)	27.3	54.8	67.7	79.6	84.7	92.3	103.9	109.3	115.8	119.7

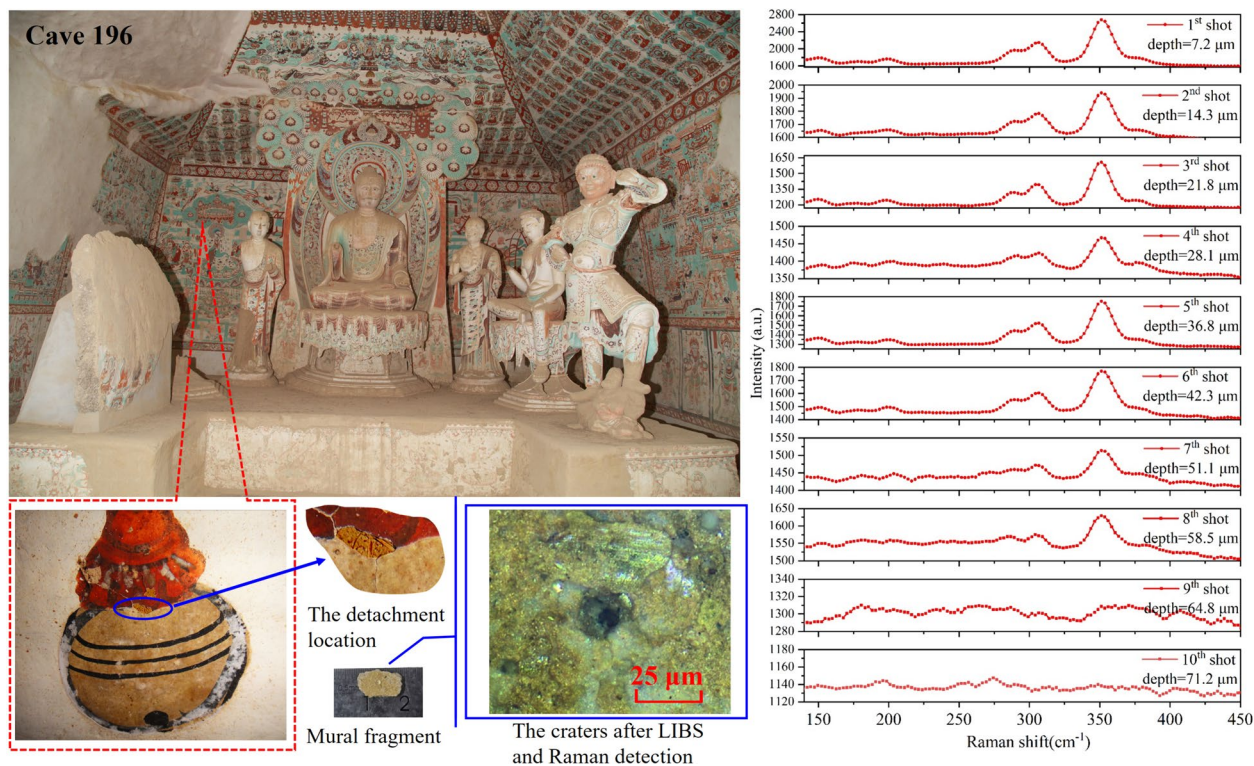


**Fig. 11** Actual mural fragment and measurement results

west wall; and Manjushri and Samantabhadra transformations on the east wall. Due to its elevated position, the cave's eave, murals, and statues remain remarkably well-preserved, exemplifying late Tang artistry.

Despite its age, Mogao Cave 196 exhibits several forms of deterioration, including flaking, detachment, powdering, alkaline efflorescence, and salt damage (Fig. 11). During ongoing restoration efforts, a mural fragment (approximately 2 cm<sup>2</sup>) detached from the pendant section of the canopy above the Buddha's head on the north wall. The largest of these fallen fragments (approximately 1.2 cm<sup>2</sup>) was analyzed using the experimental method described herein to determine pigment type and layer thickness at the detachment site.

Figure 11 details the fragment's location and presents Raman spectra before and after LIBS laser ablation. The spectra reveal orpiment as the primary pigment. After 8 laser pulses, the orpiment's Raman signal nearly vanishes. Based on the previously established average ablation rate, the orpiment layer thickness is calculated to be approximately 56.7  $\mu\text{m}$ . This aligns closely with the 58.5  $\mu\text{m}$  ablation crater depth measured using a 3D super-depth-of-field camera. It should be aware that for the pigment layer on actual mural fragment, if it is well-preserved without flaking or fading, the ablation rate measured on the mock-up block is usually very close to that measured on the actual mural. For murals that have obvious flaking and fading, the ablation rate on the mock-up block

is often different from that on the actual deteriorated fragments. In this work, the LIBS ablation rate obtained on the actual mural fragments is very close to that on the mock-up blocks because the pigment layer of these detached mural fragments is well-preserved and has not deteriorated. The primary reason for the detachment is the bulging of the ground layer. These findings demonstrate the efficacy of this experimental method in identifying pigment types and determining corresponding layer thicknesses on murals, providing critical experimental data for subsequent restoration efforts.

## Conclusions

In conclusion, this work proposes the combined use of LIBS and Raman spectroscopy for the stratigraphic analysis of murals. Through the analysis of mock-up blocks and actual mural fragment, the results confirmed that our proposed method has potential application value. The unique approach of applying both LIBS and Raman spectroscopy to the same sample points has allowed for an in-depth stratigraphic analysis of the pigment layers, distinguishing between pigments with similar elemental compositions but different molecular structures, such as orpiment and realgar. This study highlights the crucial role of non-destructive, complementary analytical techniques in the field of cultural heritage conservation, especially for sites as historically and artistically rich as the Mogao Grottoes.

Our findings demonstrate that by carefully analyzing the emission line intensity variations in LIBS spectra and correlating these with depth-specific Raman spectra, it is possible to accurately determine the composition and thickness of individual pigment layers. This method not only provides a better understanding of the materials and techniques used by the ancient artists, but also contributes to the development of more informed conservation strategies that respect the original work's integrity while protecting it for future generations.

In addition, the successful application of a computational depth-of-field camera to measure the depths of ablation craters further underscores the potential of integrating advanced imaging technologies with spectroscopic analysis for cultural heritage studies. The accuracy with which we could match the measured thicknesses of pigment layers to those anticipated on the basis of historical painting techniques validates the effectiveness of our combined analytical approach.

In essence, this work reinforces the importance of interdisciplinary collaboration in cultural heritage research, combining physics, chemistry, and art history to unveil the stories behind ancient artworks. As we continue to refine these techniques, we look forward to discovering more about the past civilizations that have shaped our cultural landscape and ensuring that their legacy is

preserved in the most authentic form possible. Our study stands as a testament to the power of modern analytical methods in bridging the gap between past and present, offering a glimpse into the artistic practices and preservation challenges of ancient muralists, with the hope that this knowledge will guide the conservation efforts of such invaluable cultural heritage sites worldwide.

## Author contributions

Duixiong and Yappeng performed experimental setup construction, data analyses, interpretation of the results emerged from both techniques and wrote the present article. Hanyun, and Guoding prepared experimental samples, performed LIBS and Raman measurements and data analyses. Maogen, Xueshi and Marek revised article, and Denghong organized these experiments.

## Funding

This work was supported by the Centrally Guided Local Development Funding Projects of China (No. 23ZYQA293), the 2024 "China-French Scientific Research Partnership Exchange Program" (51127QA), National Natural Science Foundation of China (Nos. 61965015, 12374384, 12204103), CAS Western Light Young Scholars Program (22JR9KA030), the Funds for Innovative Fundamental Research Group Project of Gansu Province (No. 22JR5RA151), Gansu Provincial Science and Technology Plan Project (No. 22JR5RA800), and the Gansu Provincial Cultural Relics Protection Science and Technology Research Project (No. GSWW202221).

## Data availability

No datasets were generated or analysed during the current study.

## Declarations

### Competing interests

The authors declare no competing interests.

### Author details

<sup>1</sup>Key Laboratory of Atomic and Molecular Physics and Functional Materials of Gansu Province, College of Physics and Electronic Engineering, Northwest Normal University, Lanzhou 730070, Gansu, China. <sup>2</sup>National Research Center for Conservation of Ancient Wall Paintings and Earthen Sites, Dunhuang 736200, China. <sup>3</sup>Centre de Recherche et de Restauration des Musées de France (C2RMF), Paris, France. <sup>4</sup>Faculty of Chemistry, Adam Mickiewicz University, 61-614 Poznań, Poland.

Received: 3 May 2024 Accepted: 16 July 2024

Published online: 25 July 2024

## References

1. Qu JJ, Cao SX, Li GS, Niu QH, Feng Q. Conservation of natural and cultural heritage in Dunhuang. *China Gondwana Res.* 2014;26:1216–21.
2. Zhang Y, Wang J, Liu H, Wang X, Zhang S. Integrated analysis of pigments on murals and sculptures in Mogao Grottoes. *Anal Lett.* 2015;48:2400–13.
3. Duan X. Study on the making materials of the wall paintings at the Mogao Grottoes. *Dunhuang Res.* 1988;3:41–59.
4. Li Y, Li B. Discussion on the technique of moving and restoring the painted murals in Grottoes. *Dunhuang Res.* 2002;4:38–44+111–15.
5. Botto A, Campanella B, Legnaioli S, Lezzerini M, Lorenzetti G, Pagnotta S, Poggialini F, Palleschi V. Applications of laser-induced breakdown spectroscopy in cultural heritage and archaeology: a critical review. *J Anal Atom Spectrom.* 2019;34:81–103.
6. Spizzichino V, Fantoni R. Laser induced breakdown spectroscopy in archeometry: a review of its application and future perspectives. *Spectrochim Acta B.* 2014;99:201–9.
7. Gaudiuso R, Dell'Aglio M, De Pascale O, Senesi GS, De Giacomo A. Laser induced breakdown spectroscopy for elemental analysis in environmental, cultural heritage and space applications: a review of methods and results. *Sensors-Basel.* 2010;10:7434–68.

8. Dell'Aglio M, Alrifai R, De Giacomo A. Nanoparticle enhanced laser induced breakdown spectroscopy (NELIBS), a first review. *Spectrochim Acta B*. 2018;148:105–12.
9. Anglos D, Couris S, Fotakis C. Laser diagnostics of painted artworks: laser-induced breakdown spectroscopy in pigment identification. *Appl Spectrosc*. 1997;5:1025–30.
10. Henry C. Taking a closer look at art. *Chem Eng News*. 2000;78:74.
11. Kaszewska EA, Sylwestrzak M, Marczak J, Skrzeczanowski W, Iwanicka M, Szmít-Naud E, Anglos D, Targowski P. Depth-resolved multilayer pigment identification in paintings: combined use of laser-induced breakdown spectroscopy (LIBS) and optical coherence tomography (OCT). *Appl Spectrosc*. 2013;67:960–72.
12. Weimerskirch MJJ, Kraft F, Pacher U, Hanneschläger G, Nagy TO. Absolute depth laser-induced breakdown spectroscopy-stratigraphy with non-scanning single spot optical coherence tomography. *Spectrochim Acta B*. 2020;172: 105916.
13. Lazić V, Vadrucchi M, Fantoni R, Chiari M. Applications of laser induced breakdown spectroscopy for cultural heritage: a comparison with X-ray fluorescence and particle induced X-ray emission techniques. *Spectrochim Acta B*. 2018;149:1–14.
14. Syvilay D, Detalle V, Wilkie-Chancellor N, Texier A, Martinez L, Serfaty S. Novel approach of signal normalization for depth profile of cultural heritage materials. *Spectrochim Acta B*. 2017;127:28–33.
15. Pospíšilová E, Novotný K, Pořízka P, Hradil D, Hradilová J, Kaiser J, Kanický V. Depth-resolved analysis of historical painting model samples by means of laser-induced breakdown spectroscopy and handheld X-ray fluorescence. *Spectrochim Acta B*. 2018;147:100–8.
16. Veneranda M, Prieto-Taboada N, Fdez-Ortiz de Vallejuelo S, Maguregui M, Morillas H, Marcaida I, Castro K, Garcia-Diego F-J, Osanna M, Madariaga JM. In-situ multi analytical approach to analyze and compare the degradation pathways jeopardizing two murals exposed to different environments (Ariadne House, Pompeii, Italy). *Spectrochim Acta B*. 2018;203:201–9.
17. Kaszewska EA, Sylwestrzak M, Marczak J, Skrzeczanowski W, Iwanicka M, Szmít-Naud E, Anglos D, Targowski P. Depth-resolved multilayer pigment identification in paintings: combined use of laser-induced breakdown spectroscopy (LIBS) and optical coherence tomography (OCT). *Appl Spectrosc*. 2013;67:960–72.
18. Vandenaabeele P, Edwards HGM, Moens L. A Decade of Raman spectroscopy in art and archaeology. *Chem Rev*. 2007;3:675–86.
19. Vandenaabeele P. Raman spectroscopy in art and archaeology. *J Raman Spectrosc*. 2007;35:607–9.
20. Coupry C, Lauté A, Revault M, Dufilho J. Contribution of Raman spectroscopy to art and history. *J Raman Spectrosc*. 1994;25:89–94.
21. Baraldi P, Tinti A. Raman spectroscopy in art and archaeology. *J Raman Spectrosc*. 2008;39:963–5.
22. Fau A, Beyssac O, Gauthier M, Meslin PY, Cousin A, Benzerara K, Bernard S, Boulliard JC, Gasnault O, Forni O, Wiens RC, Morand M, Rosier P, Garino Y, Pont S, Maurice S. Pulsed laser-induced heating of mineral phases: Implications for Laser-Induced Breakdown Spectroscopy combined with Raman spectroscopy. *Spectrochim Acta B*. 2019;160: 105687.
23. Toschi F, Paladini A, Colosi F, Cafarelli P, Valentini V, Falconieri M, Gagliardi S, Santoro P. A multi-technique approach for the characterization of Roman mural paintings. *Appl Surf Sci*. 2013;284:291–6.
24. Gebremariam KF, Kvittingen L, Nicholson DG. Multi-analytical investigation into painting materials and techniques: the wall paintings of Abuna Yemata Guh church. *Herit Sci*. 2016;4:1–14.
25. Colombari P. On-site Raman study of artwork: procedure and illustrative examples. *J Raman Spectrosc*. 2018;49:921–34.
26. Colombari P. The on-site/remote Raman analysis with mobile instruments: a review of drawbacks and success in cultural heritage studies and other associated fields. *J Raman Spectrosc*. 2012;43:1529–35.
27. Vandenaabeele P, Edwards HGM, Jehlička J. The role of mobile instrumentation in novel applications of Raman spectroscopy: archaeometry, geosciences, and forensics. *Chem Soc Rev*. 2014;43:2628–49.
28. Ciofini D, Agresti J, Mencaglia AA, Siano S, Osticioli I. Temperature sensing during Raman spectroscopy of lead white films in different purity grades and boundary conditions. *Sensor Actuat B-Chem*. 2020;325:128958.
29. Etxebarria I, Prieto-Taboada N, Lama E, Arana G, Rodríguez-Laso MD, Madariaga JM. Graffiti characterization prior to intervention in the Punta Begoña Galleries (Getxo, north of Spain): Raman and XRF spectroscopy in the service of restoration. *Appl Sci*. 2021;11:8640.
30. Zheng YX, He X, Li X, Chen KL, Guo H, Pan XX. Raman spectroscopy analysis of the mural pigments in Lam Rim Hall of Wudang Lamasery, Baotou Area, Inner Mongolia. *China Minerals*. 2022;12:456.
31. Veneranda M, Irazola M, Díez M, Iturregui A, Aramendia J, Castro K, Madariaga JM. Raman spectroscopic study of the degradation of a middle age mural painting: the role of agricultural activities. *J Raman Spectrosc*. 2014;45:1110–8.
32. Chiriu D, Desogus G, Pisu FA, Fiorino DR, Grillo SM, Ricci PC, Carbonaro CM. Beyond the surface: Raman micro-SORS for in depth non-destructive analysis of fresco layers. *Microchem J*. 2020;153: 104404.
33. Tournon S, Trichereau B, Syvilay D. In-depth analyses of paleolithic pigments in cave climatic conditions. *Optical Metrology*. 2017;10331:112–20.
34. Bruder R, Detalle V, Coupry C. An example of the complementarity of laser-induced breakdown spectroscopy and Raman microscopy for wall painting pigments analysis. *J Raman Spectrosc*. 2007;38:909–15.
35. Glaus R, Hahn DW. Fiber-coupled laser-induced breakdown and Raman spectroscopy for flexible sample characterization with depth profiling capabilities. *Spectrochim Acta B*. 2014;100:116–22.
36. Paladini A, Toschi F, Colosi F, Santoro P, Rubino G. Stratigraphic investigation of wall painting fragments from Roman villas of the Sabina area. *Appl Phys A*. 2015;118:131–8.
37. Bicchiari M, Nardone M, Russo PA, Sodo A, Corsi M, Cristoforetti G, Palleschi V, Salvetti A, Tognoni E. Characterization of azurite and lazurite based pigments by laser induced breakdown spectroscopy and micro-Raman spectroscopy. *Spectrochim Acta B*. 2001;56:915–22.
38. Castillejo M, Martín M, Silva D, Stratoudaki T, Anglos D, Burgio L, Clark RJH. Analysis of pigments in polychromes by use of laser induced breakdown spectroscopy and Raman microscopy. *J Mol Struct*. 2000;550–551:191–98.
39. Veneranda M, Prieto-Taboada N, Fdez-Ortiz de Vallejuelo S, Maguregui M, Morillas H, Marcaida I, Castro K, Garcia-Diego F-J, Osanna M, Madariaga JM. In-situ multianalytical approach to analyze and compare the degradation pathways jeopardizing two murals exposed to different environments (Ariadne House, Pompeii, Italy). *Spectrochim Acta B*. 2018;203:201–9.
40. Burgio L, Melessanaki K, Doulgeridis M, Clark RJH, Anglos D. Pigment identification in paintings employing laser induced breakdown spectroscopy and Raman microscopy. *Spectrochim Acta B*. 2001;56:905–13.
41. Osticioli I, Mendes NFC, Porcinai S, Cagnini A, Castellucci E. Spectroscopic analysis of works of art using a single LIBS and pulsed Raman setup. *Anal Bioanal Chem*. 2009;394:1033–41.
42. Yu ZR, Sun BN, Fan YQ, Su BM. A preliminary study on the yellow pigment of Yuan Dynasty murals in Yulin Grottoes. *Dunhuang Res*. 2008;6:46–9.
43. Shi Li. A preliminary understanding of cementing materials in Dunhuang murals. *Dunhuang Res*. 1993;1:108–17.
44. Vitková G, Prokeš L, Novotný K, Čelko L, Pořízka P, Novotný J, Všianský D, Kaiser J. Comparative study on fast classification of brick samples by combination of principal component analysis and linear discriminant analysis using stand-off and table-top laser-induced breakdown spectroscopy. *Spectrochim Acta B*. 2014;101:191–9.
45. Yin YP, Yu ZR, Sun DX, Su MG, Wang Z, Shan ZW, Han WW, Su BM, Dong CZ. A potential method to determine pigment particle size on ancient murals using laser induced breakdown spectroscopy and chemometric analysis. *Anal Methods*. 2021;13:1381–91.
46. Guezenc J, Gallet-Budynek A, Bousquet B. Critical review and advices on spectral-based normalization methods for LIBS quantitative analysis. *Spectrochim Acta B*. 2019;160: 105688.
47. Chen K, Leona M, Vo-Dinh T. Surface-enhanced Raman scattering for identification of organic pigments and dyes in works of art and cultural heritage material. *Sensor Rev*. 2007;27:109–20.
48. Frost RL, Martens WN, Klopogge JT. Raman spectroscopic study of cinnabar(HgS), realgar(As<sub>2</sub>S<sub>4</sub>), and orpiment(As<sub>2</sub>S<sub>3</sub>) at 298 and 77 K. *Neues Jahrbuch für Mineralogie Monatshefte*. 2002;10:469–80.

## Publisher's Note

Springer Nature remains neutral with regard to jurisdictional claims in published maps and institutional affiliations.